Computational Simulations and Experiments on Vibration Control of a Flexible Two-link Manipulator Using a Piezoelectric Actuator

Abdul Kadir Muhammad, Shingo Okamoto, Jae Hoon Lee, *Members, IAENG*

***Abstract*— The purposes of this research are to formulate the equations of motion of a flexible two-link system, to develop computational codes by a finite-element method in order to perform dynamics simulations with vibration control, to propose an effective control scheme and to confirm the calculated results by experiments of a flexible two-link manipulator. The system used in this paper consists of two aluminum beams as flexible links, two clamp-parts, two servo motors to rotate the links and a piezoelectric actuator to control vibration. Computational codes on time history responses, FFT (Fast Fourier Transform) processing and eigenvalues - eigenvectors analysis were developed to calculate the dynamic behavior of the links. Furthermore, a control scheme using a piezoelectric actuator was designed to suppress the vibration. A proportional-derivative (PD) control was designed and demonstrated its performances. The system and the proposed control scheme were confirmed through experiments. The calculated and experimental results revealed that the vibration of the flexible two-link manipulator can be controlled effectively.**

***Index Terms*—Finite-element method, flexible manipulator, piezoelectric actuator, vibration control.**

I. Introduction

EMPLOYMENT of flexible link manipulator is recommended in the space and industrial applications in order to accomplish high performance requirements such as high-speed besides safe operation, increasing of positioning accuracy and lower energy consumption, namely less weight. However, it is not usually easy to control a flexible manipulator because of its inheriting flexibility. Deformation of the flexible manipulator when it is operated must be considered by any control. Its controller system should be dealt with not only its motion but also vibration due to the flexibility of the link.

In the past few decades, a number of modeling methods and control strategies using piezoelectric actuators to deal with the vibration problem have been investigated by researchers [1 – 10]. Nishidome and Kajiwara [1] investigated a way to enhance performances of motion and vibration of a flexible-link mechanism. They used a modeling method based on modal analysis using the finite-element method. The model was described as a state space form. Their control system was constructed with a designed dynamic compensator based on the mixed of H_2/H_∞. They recommended separating the motion and vibration controls of the system. Yavus Yaman et al [2] and Kircali et al [3] studied an active vibration control technique on aluminum beam modeled in cantilevered configuration. The studies used the ANSYS package program for modeling. They investigated the effect of element selection in finite-element modeling. The model was reduced to state space form suitable for application of H_∞ [2] and spatial H_∞ [3] controllers to suppress vibration of the beam. They showed the effectiveness of their techniques through simulation. Zhang et al [4] has studied a flexible piezoelectric cantilever beam. The model of the beam using finite-elements was built by ANSYS application. Based on the Linear Quadratic Gauss (LQG) control method, they introduced a procedure to suppress the vibration of the beam with the piezoelectric sensors and actuators were symmetrically collocated on both sides of the beam. Their simulation results showed the effectiveness of the method. Gurses et al [5] investigated vibration control of a flexible single-link manipulator using three piezoelectric actuators. The dynamic modeling of the link had been presented using Euler-Bernoulli beam theory. Composite linear and angular velocity feedback controls were introduced to suppress the vibration. Their simulation and experimental results showed the effectiveness of the controllers. Xu and Koko [6] studied finite-element analysis and designed controller for flexible structures using piezoelectric material as actuators and sensors. They used a commercial finite-element code for modeling and completed with an optimal active vibration control in state space form. The effectiveness of the control method was confirmed through simulations. Kusculuoglu et al [7] had used a piezoelectric actuator for excitation and control vibrations of a beam. The beam and actuator were modeled using Timoshenko beam theory. An optimized vibration absorber using an electrical resistive-inductive shun circuit on the actuator was used as a passive controller. The effectiveness of results was shown by simulations and experiment.

Furthermore, Hewit et al [8] used the Active-force (AF) control for deformation and disturbance attenuation of a flexible manipulator. Then, a PD control was used for trajectory tracking of the flexible manipulator. They used a motor as an actuator. Modeling of the manipulator was done using virtual link coordinate system (VLCS). Their simulation results had shown that the proposed control could cancel the disturbance satisfactorily. Tavakolvour et al [9] investigated the AF control application for a flexible thin plate. Modeling of their system was done using

Manuscript received April 30, 2015; revised May 21, 2015.
Every author is with Mechanical Engineering Course, Graduate School of Science and Engineering, Ehime University, 3 Bunkyo-cho, Matsuyama 790-8577, Japan. (e-mail: y861008b@mails.cc.ehime-u.ac.jp, kadir_muhammad@yahoo.co.id, okamoto.shingo.mh@ehime-u.ac.jp, jhlee@ehime-u.ac.jp).

The first author is also with Center for Mechatronics and Control System, Mechanical Engineering Department, State Polytechnic of Ujung Pandang, Jl. Perintis Kemerdekaan KM 10 Makassar, 90-245, Indonesia.

finite-difference method. Their calculated results showed the effectiveness of the proposed controller to reduce vibration of the plate. Tavakolvour and Mailah [10] studied the AF control application for a flexible beam with an electromagnetic actuator. Modeling of the beam was done using finite-difference method. The effectiveness of the proposed controller was confirmed through simulation and experiment.

In the recent two years, Muhammad et al [11 – 15] have actively studied vibration control on a flexible single-link manipulator with a piezoelectric actuator using finite-element method. Model of the single-link and the piezolecetric actuator was built using one-dimensional and two-node elements. They introduced a simple and effective control scheme with the actuator using proportional (P), PD and AF controls strategies. The effectivenesses of the proposed control scheme and strategies were shown through simulations and experiments.

The purposes of this research are to derive the equations of motion of a flexible two-link system by a finite-element method, to develop computational codes in order to perform dynamics simulations with vibration control and to propose an effective control scheme of a flexible two-link manipulator.

The flexible two-link manipulator used in this paper consists of two aluminum beams as flexible links, two aluminum clamp-parts, two servo motors to rotate the links and a piezoelectric actuator to control vibration. Computational codes on time history responses, FFT (Fast Fourier Transform) processing and eigenvalues - eigenvectors analysis were developed to calculate the dynamic behavior of the links. Finally, a PD controller was designed to suppress the vibration. It was done by adding bending moments generated by the piezoelectric actuators to the two-link system.

II. Formulation by Finite-element Method

The links have been discretized by finite-elements. Every finite-element (Element *i*-th) has two nodes namely Node *i* and Node (*i*+1). Every node (Node *i*) has two degrees of freedom [11 – 15], namely the lateral deformation $v_i(x,t)$, and the rotational angle $\psi_i(x,t)$. The length, the cross-sectional area and the area moment of inertia around *z*-axis of every element are denoted by l_i, S_i and I_{zi} respectively. Mechanical properties of every element are denoted as Young's modulus E_i and mass density ρ_i.

A. Kinematic

Figure 1 shows the position vectors $\boldsymbol{r}_{p1}$ and $\boldsymbol{r}_{p2}$ of arbitrary points P_1 and P_2 on Link 1 and Link 2 in the global and rotating coordinate frames. Let the links as flexible beams have a motion that is confined in the horizontal plane as shown in Fig. 1. The $O - XY$ frame is the global coordinate frame with *Z*-axis is fixed. Furthermore, $o_1 - x_1y_1$ and $o_2 - x_2y_2$ are the rotating coordinate frames fixed to the root of Link 1 and Link 2, respectively (z_1-axis and z_2-axis are fixed). The unit vectors in *X*, *Y*, x_1, y_1, x_2 and y_2 axes are denoted by $\boldsymbol{I}$, $\boldsymbol{J}$, $\boldsymbol{i}_1$, $\boldsymbol{j}_1$, $\boldsymbol{i}_2$ and $\boldsymbol{j}_2$, respectively. The first motor is installed on the root of the Link 1. The second motor that treated as a concentrated mass is installed in the root of the Link 2. The rotational angles of the first and second motor when the links rotate are denoted by $\theta_1(t)$ and $\theta_2(t)$. Length of Link 1 is donated by L_1. Lateral deformation of the arbitrary points P_1 and P_2 in the first and the second links are donated by v_{p1} and v_{p2}, respectively. Lateral deformation and rotational angel of the end-point of the first link are donated by v_e and ψ_e, respectively. The position vectors $\boldsymbol{r}_{p1}$ and $\boldsymbol{r}_{p2}$ of the arbitrary points P_1 and P_2 at time $t = t$, measured in the $O - XY$ frame shown in Fig. 1 are expressed by

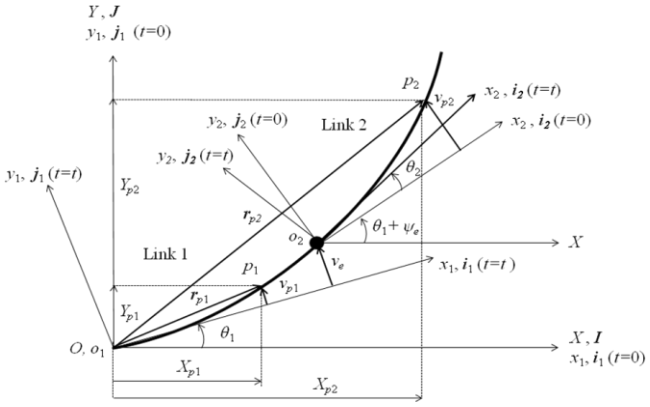

O-XY : Global coordinate frame
o_1-x_1y_1 : Rotating coordinate frame fixed to Link 1
o_2-x_2y_2 : Rotating coordinate frame fixed to Link 2
$\boldsymbol{r}_{p1}$, $\boldsymbol{r}_{p2}$: Position vectors of the arbitrary points p_1 and p_2 in the *O-XY*
θ_1 : Rotational angle of the first motor
θ_2 : Rotational angle of the second motor
X_{p1}, X_{p2} : Coordinates of the arbitrary points p_1 and p_2 in the *X*-axis of the *O-XY*
Y_{p1}, Y_{p2} : Coordinates of the arbitrary points p_1 and p_2 in the *Y*-axis of the *O-XY*
v_{p1} : Lateral deformation of the arbitrary point p_1 on Link 1 in the o_1-x_1y_1
v_{p2} : Lateral deformation of the arbitrary point p_2 on Link 2 in the o_2-x_2y_2
ψ_e : Rotational angle of the end-point of Link 1
v_e : Lateral deformation of the end-point of Link 1
L_1 : Length of Link 1

Fig. 1. Position vectors of arbitrary points P_1 and P_2 in the global and rotating coordinate frames

$$\boldsymbol{r}_{p1} = X_{p1}(x_1,\theta_1,v_{p1},t)\boldsymbol{I} + Y_{p1}(x_1,\theta_1,v_{p1},t)\boldsymbol{J} \quad (1)$$

$$\boldsymbol{r}_{p2} = X_{p2}(x_2,\theta_1,\theta_2,v_e,\psi_e,v_{p2},t)\boldsymbol{I} + Y_{p2}(x_2,\theta_1,\theta_2,v_e,\psi_e,v_{p2},t)\boldsymbol{J} \quad (2)$$

Where

$$X_{p1} = x_1\cos\theta_1(t) - v_{p1}(x_1,t)\sin\theta_1(t) \quad (3)$$

$$Y_{p1} = x_1\sin\theta_1(t) + v_{p1}(x_1,t)\cos\theta_1(t) \quad (4)$$

$$X_{p2} = L_1\cos\theta_1(t) - v_e(x_1,t)\sin\theta_1(t) + x_2\cos\big(\theta_1(t)+\psi_e(x_1,t)+\theta_2(t)\big) - v_{p2}(x_2,t)\sin\big(\theta_1(t)+\psi_e(x_1,t)+\theta_2(t)\big) \quad (5)$$

$$Y_{p2} = L_1\sin\theta_1(t) + v_e(x_1,t)\cos\theta_1(t) + x_2\sin\big(\theta_1(t)+\psi_e(x_1,t)+\theta_2(t)\big) + v_{p2}(x_2,t)\cos\big(\theta_1(t)+\psi_e(x_1,t)+\theta_2(t)\big) \quad (6)$$

The velocity vectors of the arbitrary points P_1 and P_2 at time $t = t$, shown in Fig.1 are expressed by

$$\dot{\boldsymbol{r}}_{p1} = \dot{X}_{p1}(x_1,\theta_1,\dot{\theta}_1,v_{p1},\dot{v}_{p1},t)\boldsymbol{I} + \dot{Y}_{p1}(x_1,\theta_1,\dot{\theta}_1,v_{p1},\dot{v}_{p1},t)\boldsymbol{J} \quad (7)$$

$$\dot{\boldsymbol{r}}_{p2} = \dot{X}_{p2}(x_2,\theta_1,\theta_2,\dot{\theta}_1,\dot{\theta}_2,v_e,\psi_e,v_{p2},\dot{v}_e,\dot{\psi}_e,\dot{v}_{p2},t)\boldsymbol{I} + \dot{Y}_{p1}(x_2,\theta_1,\theta_2,\dot{\theta}_1,\dot{\theta}_2,v_e,\psi_e,v_{p2},\dot{v}_e,\dot{\psi}_e,\dot{v}_{p2},t)\boldsymbol{J} \quad (8)$$

B. Finite-element Method

Figure 2 shows the element coordinate frame of Element *i*, and an arbitrary point *P* on Element *i*. Here, there are four boundary conditions together at nodes *i* and (*i*+1) when the one-dimensional and two-node element is used. The four boundary conditions are expressed as nodal vector as follow

$$\boldsymbol{\delta}_i = \{v_i \quad \psi_i \quad v_{i+1} \quad \psi_{i+1}\}^T \quad (9)$$

Then, the hypothesized deformation has four constants as follows [16]

$$v_i = a_1 + a_2 x_i + a_3 {x_i}^2 + a_4 {x_i}^3 \quad (10)$$

where x_i is position coordinate of the arbitrary point *P* in the x_i-axis of the element coordinate frame.

Then, the relation between the lateral deformation v_i and the rotational angle ψ_i of the Node *i* is given by

$$\psi_i = \frac{\partial v_i}{\partial x_i} \quad (11)$$

Moreover, from mechanics of materials, the strain of Node *i* can be defined by

$$\varepsilon_i = -y_i \frac{\partial^2 v_i}{\partial {x_i}^2} \quad (12)$$

where y_i is position coordinate of the arbitrary point *P* in the y_i-axis of the element coordinate frame.

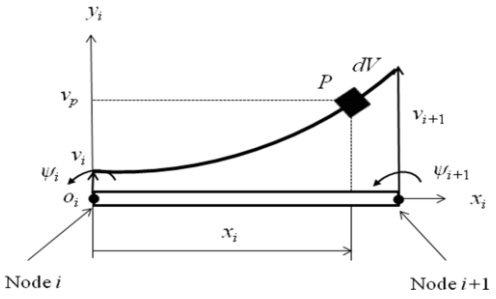

$o_i - x_i\, y_i$: Element coordinate frame of the Element *i*

Fig. 2. Element coordinate frame of the Element *i*

C. Equations of motion

Equations of motion of Element *i*-th on Link 1 and Link 2 are respectively given by

$$\boldsymbol{M}_i\ddot{\boldsymbol{\delta}}_i + \boldsymbol{C}_i\dot{\boldsymbol{\delta}}_i + \left[\boldsymbol{K}_i - {\dot{\theta}_1}^2 \boldsymbol{M}_i\right]\boldsymbol{\delta}_i = \ddot{\theta}_1 \boldsymbol{f}_i \quad (13)$$

$$\boldsymbol{M}_i\ddot{\boldsymbol{\delta}}_i + \boldsymbol{C}_i\dot{\boldsymbol{\delta}}_i + \left[\boldsymbol{K}_i - \left(\dot{\theta}_1 + \dot{\psi}_e + \dot{\theta}_2\right)^2 \boldsymbol{M}_i\right]\boldsymbol{\delta}_i = \left(\ddot{\theta}_1 + \ddot{\psi}_e + \ddot{\theta}_2\right)\boldsymbol{f}_i + \left(L_1\ddot{\theta}_1 + \ddot{v}_e - v_e{\dot{\theta}_1}^2\right)\cos(\psi_e + \theta_2)\boldsymbol{g}_i + \left(v_e\ddot{\theta}_1 + L_1{\dot{\theta}_1}^2 + \frac{1}{2}\dot{v}_e\left(3\dot{\theta}_1 - \dot{\psi}_e - \dot{\theta}_2\right)\right)\sin(\psi_e + \theta_2)\boldsymbol{g}_i \quad (14)$$

where $\boldsymbol{M}_i$, $\boldsymbol{C}_i$, and $\boldsymbol{K}_i$, are the mass matrix, damping matrix, stiffness matrix of Element *i* on Link 1 and Link 2. Vectors of $\boldsymbol{f}_i$ and $\boldsymbol{g}_i$ are the excitation vectors on Link 1 and Link 2. The representation of the matrices and the vector of $\boldsymbol{f}_i$ can be found in [11] and [13]. The vector of $\boldsymbol{g}_i$ can be defined by

$$\boldsymbol{g}_i = \frac{\rho_i S_i l_i}{12}\{-6 \quad 15l_i \quad 6 \quad l_i\}^T \quad (15)$$

Finally, the equations of motion of Link 1 and Link 2 with *n* elements considering the boundary conditions is respectively given by

$$\boldsymbol{M}_n\ddot{\boldsymbol{\delta}}_n + \boldsymbol{C}_n\dot{\boldsymbol{\delta}}_n + \left[\boldsymbol{K}_n - {\dot{\theta}_1}^2 \boldsymbol{M}_n\right]\boldsymbol{\delta}_n = \ddot{\theta}_1 \boldsymbol{f}_n \quad (16)$$

$$\boldsymbol{M}_n\ddot{\boldsymbol{\delta}}_n + \boldsymbol{C}_n\dot{\boldsymbol{\delta}}_n + \left[\boldsymbol{K}_n - \left(\dot{\theta}_1 + \dot{\psi}_e + \dot{\theta}_2\right)^2 \boldsymbol{M}_n\right]\boldsymbol{\delta}_n = \left(\ddot{\theta}_1 + \ddot{\psi}_e + \ddot{\theta}_2\right)\boldsymbol{f}_n + \left(L_1\ddot{\theta}_1 + \ddot{v}_e - v_e{\dot{\theta}_1}^2\right)\cos(\psi_e + \theta_2)\boldsymbol{g}_n + \left(v_e\ddot{\theta}_1 + L_1{\dot{\theta}_1}^2 + \frac{1}{2}\dot{v}_e\left(3\dot{\theta}_1 - \dot{\psi}_e - \dot{\theta}_2\right)\right)\sin(\psi_e + \theta_2)\boldsymbol{g}_n \quad (17)$$

III. Validation of Formulation and Computational Codes

A. Experimental Model

Figure 3 shows the experimental model of the flexible two-link manipulator. The flexible manipulator consists of two flexible aluminum beams, two clamp-parts, two servo motors and the base. Link 1 and Link 2 are attached to the first and second motors through the clamp-parts. Link 1 and Link 2 are connected through the second motor. Two strain gages are bonded to the position of 0.11 [m] and 0.38 [m] from the origin of the two-link system. The first motor is mounted to the base. In the experiments, the motors were operated by an independent motion controller.

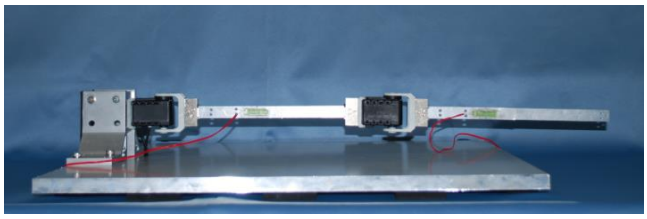

Fig. 3. Experimental model of the flexible two-link manipulator

B. Computational Models

In this research, we defined and used three types of computational models of the flexible two-link manipulator.

Model A

A model of only a two-link manipulator was used as Model *A*. Figure 4.a shows Model *A*. The links and the clamp-parts were discretized by 35 elements. Two strain gages are

bonded to the position of Node 6 and Node 22 of the two-link (0.11 [m] and 0.38 [m] from the link's origin), respectively.

Model B

A model of the flexible two-link manipulator including a piezoelectric actuator was defined as Model *B*. Figure 4.b shows Model *B*. The piezoelectric actuator was bonded to the one surface of Elements 4. The links including the clamp-parts and the piezoelectric actuator were discretized by 36 elements. Schematic representations on modeling of the piezoelectric actuators are shown in Fig. 5. Physical parameters of the flexible two-link manipulator models and the piezoelectric actuator are shown in table 1.

The piezoelectric actuator suppresses the vibration of the two-link flexible manipulator by adding bending moments at Nodes 3 and 6 of the two-link manipulator, M_3 and M_6. The bending moments are generated by applying voltages E to the piezoelectric actuator. The bending moments proportional to the voltage which are expressed by

$$M_3 = -M_6 = d_1 E \tag{18}$$

Here d_1 is a constant quantity and M_3 opposites to M_6.

Furthermore, the voltage to generate the bending moments is proportional to the strain measured by the first strain gage, ε_1 of the two-link due to the vibration. The relation can be expressed as follows

$$E = \frac{1}{d_2}\varepsilon_1 \tag{19}$$

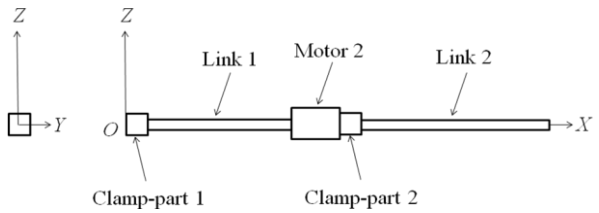

(a) Model *A*: Only two-link

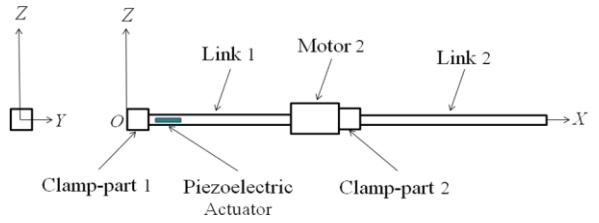

(b) Model *B*: Two-link with a piezoelectric actuator

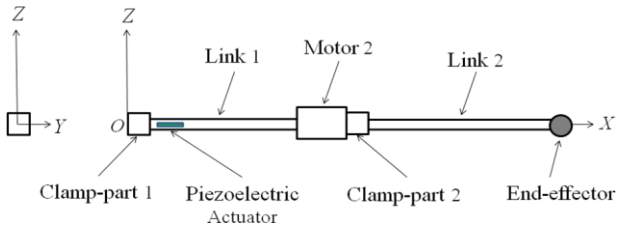

(b) Model *C*: Two-link with a piezoelectric actuator and an end-effector

Fig. 4. Computational models of the flexible two-link manipulator

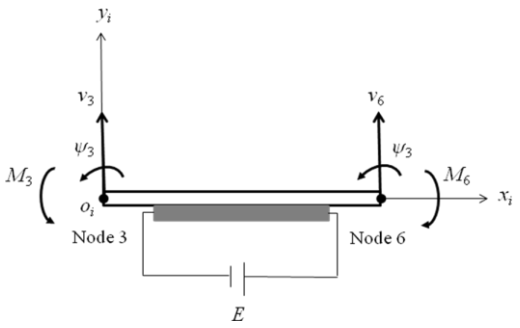

Fig. 5. Modeling of the piezoelectric actuator

TABLE I
PHYSICAL PARAMETERS OF THE FLEXIBLE LINK AND THE PIEZOELECTRIC ACTUATOR [17]

l	Total length	m	4.05×10^{-1}
l_1	Length of Link 1	m	1.90×10^{-1}
l_2	Length of Link 2	m	2.15×10^{-1}
l_{c1}, l_{c2}	Length of clamp-parts 1 and 2	m	1.50×10^{-2}
l_{a1}, l_{a2}	Length of Actuators 1 and 2	m	2.00×10^{-2}
S_{l1}, S_{l2}	Cross section area of links 1 and 2	m^2	1.95×10^{-5}
S_{c1}, S_{c2}	Cross section area of clamp-parts 1 and 2	m^2	8.09×10^{-4}
S_{a1}, S_{a2}	Cross section area of actuators 1 and 2	m^2	1.58×10^{-5}
I_{zl1}, I_{zl2}	Cross section area moment of inertia around z-axis of links 1 and 2	m^4	2.75×10^{-12}
I_{zc1}, I_{zc2}	Cross section area moment of inertia around z-axis of clamp-parts 1 and 2	m^4	3.06×10^{-8}
I_{za1}, I_{za2}	Cross section area moment of inertia around z-axis of actuators 1 and 2	m^4	1.61×10^{-11}
E_{l1}, E_{l2}	Young's Modulus of links 1 and 2	GPa	7.03×10^{1}
E_{c1}, E_{c2}	Young's Modulus of clamp-parts 1 and 2	GPa	7.03×10^{1}
E_{a1}, E_{a2}	Young's Modulus of actuators 1 and 2	GPa	4.40×10^{1}
ρ_{l1}, ρ_{l2}	Density of links 1 and 2	kg/m^3	2.68×10^{3}
ρ_{c1}, ρ_{c2}	Density of clamp-parts 1 and 2	kg/m^3	2.68×10^{3}
ρ_{a1}, ρ_{a2}	Density of actuators 1 and 2	kg/m^3	3.33×10^{3}
α_1, α_2	Damping factor of links 1 and 2	s	2.50×10^{-4}
E_1, E_2	Maximum input voltages of actuators 1 and 2	V	150.00
F_1, F_2	Maximum output forces of actuators 1 and 2	N	200.00
m_2	Mass of the second motor and it's clamping system	g	113.53

Here d_2 is a constant quantity. Then, d_1 and d_2 will be determined by comparing the calculated results and experimental ones.

Model C

Figure 4.c shows model *C* that an end-effector is considered for a two-link manipulator with a piezoelectric actuator. Model *C* is used to show that the proposed control scheme is also suitable for such system. The end-effector is presented by adding a concentrated mass to Model *B*. In this case, the equation of motion of the tip element containing the concentrated mass is given by

$$\left[\boldsymbol{M}_i + \boldsymbol{M}_{icm}\right]\ddot{\boldsymbol{\delta}}_i + \boldsymbol{C}_i\dot{\boldsymbol{\delta}}_i + \left[\boldsymbol{K}_i - \left(\dot{\theta}_1 + \dot{\psi}_e + \dot{\theta}_2\right)^2\left[\boldsymbol{M}_i + \boldsymbol{M}_{icm}\right]\right]\boldsymbol{\delta}_i = \left(\ddot{\theta}_1 + \ddot{\psi}_e + \ddot{\theta}_2\right)\left\{\boldsymbol{f}_i + \boldsymbol{f}_{icm}\right\} + \left(L_1\ddot{\theta}_1 + \ddot{v}_e - v_e\dot{\theta}_1^{\,2}\right)\cos\left(\psi_e + \theta_2\right)\left\{\boldsymbol{g}_i + \boldsymbol{g}_{icm}\right\} + \left(v_e\ddot{\theta}_1 + L_1\dot{\theta}_1^{\,2} + \frac{1}{2}\dot{v}_e\left(3\dot{\theta}_1 - \dot{\psi}_e - \dot{\theta}_2\right)\right)\sin\left(\psi_e + \theta_2\right)\left\{\boldsymbol{g}_i + \boldsymbol{g}_{icm}\right\} \quad (20)$$

where the vectors of $\boldsymbol{f}_{icm}$ and $\boldsymbol{g}_{icm}$ are respectively given by

$$\boldsymbol{f}_{icm} = -m_c\left\{0 \quad 0 \quad -l_{1-i} - l_i \quad 0\right\}^T \quad (21)$$

$$\boldsymbol{g}_{icm} = -m_c\left\{0 \quad 0 \quad -1 \quad 0\right\}^T \quad (22)$$

and the concentrated mass matrix M_{icm} can be expressed as

$$\boldsymbol{M}_{icm} = \begin{bmatrix} 0 & 0 & 0 & 0 \\ 0 & 0 & 0 & 0 \\ 0 & 0 & m_c & 0 \\ 0_i & 0 & 0 & 0 \end{bmatrix} \quad (23)$$

where m_c is the mass of the concentrated mass.

C. Time History Responses of Free Vibration

Experiment on free vibration was conducted using an impulse force as an external one. Figure 6 shows the experimental time history response of strains, ε_e on the free vibration at the same position in the calculation (0.11 [m] from the origin of the two-link system). Furthermore, the computational codes on time history response of Model *A* were developed. Figure 7 shows the calculated strains at Node 6 of Model *A* under the impulse force.

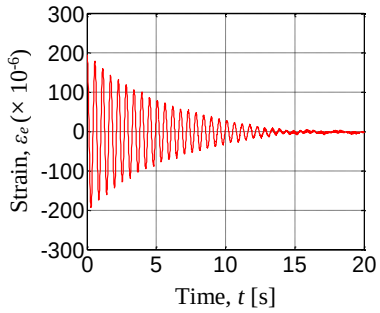

Fig. 6. Experimental time history response of strains on free vibration of the flexible two-link at 0.11 [m] from the origin of the two-link

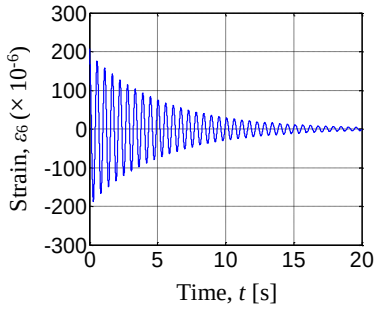

Fig. 7. Calculated time history response of strains on free vibration at Node 6 of Model *A*

D. Fast Fourier Transform (FFT) Processing

Both the experimental and calculated time history responses on free vibration were transferred by FFT processing to find their frequencies.

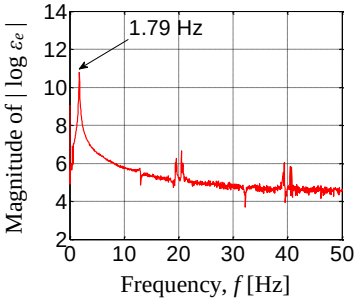

Fig. 8. Experimental natural frequency of the flexible two-link

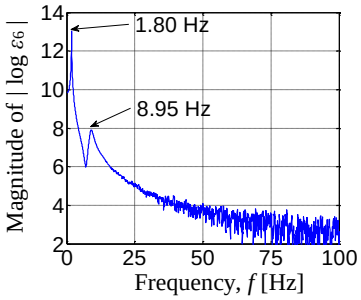

Fig. 9. Calculated natural frequencies of Model *A*

Figures 8 and 9 show the experimental and calculated natural frequencies of the flexible two-link manipulator, respectively. The first experimental natural frequency, 1.79 [Hz] agreed with the calculated one, 1.80 [Hz]. The second experimental natural frequency could not be measured. However, it could be obtained as 8.95 [Hz] in the calculation.

E. Eigen-values and Eigen-vectors Analysis

The computational codes on Eigen-values and Eigen-vectors analysis were developed for natural frequencies and vibration modes.

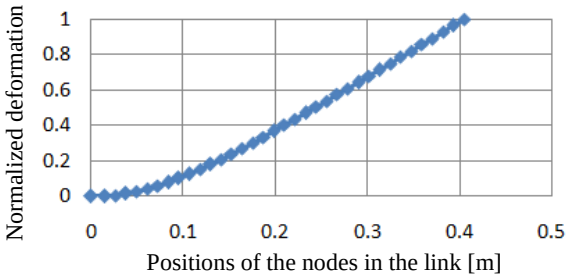

Fig. 10. First vibration mode and natural frequency (f_1 = 1.79 [Hz]) of Model *A*

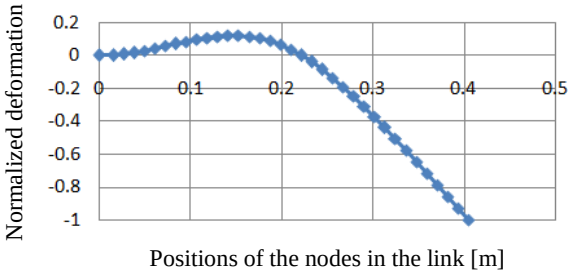

Fig. 11. Second vibration mode and natural frequency (f_2 = 8.92 [Hz]) of Model *A*

The calculated results for the first and second natural frequencies were 1.79 [Hz] and 8.92 [Hz], respectively. The vibration modes of natural frequencies are shown in Figures 10 and 11.

F. Time History Responses due to Base Excitation

Another experiment was conducted to investigate the vibration of the flexible two-link due to the base excitation generated by rotation of the motor. In the experiment, the first motor were rotated by the angle of $\pi/2$ radians (90 degrees) within 0.50 [s]. Figures 12 and 14 show the experimental time history responses of strains of the flexible two-link due to the motor' rotation at 0.11 [m] and 0.38 [m] from the origin of the link, respectively. Furthermore, based on Figures 12 and 14, the time history responses of strains at Node 6 and Node 22 of Model *A* were calculated as shown in Figures 13 and 15, respectively.

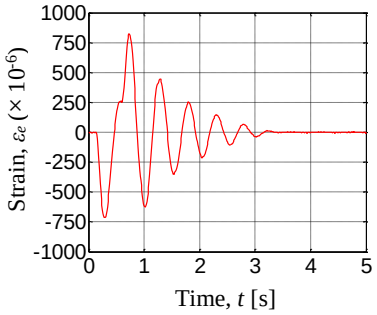

Fig. 12. Experimental time history responses of strains at 0.11 [m] from the origin of the two-link due to the base excitation

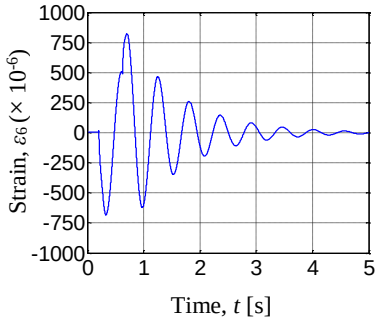

Fig. 13. Calculated time history responses of strains at Node 6 of Model *A* due to the base excitation

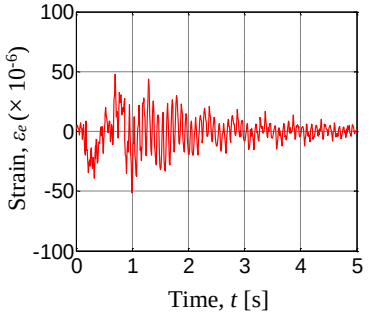

Fig. 14. Experimental time history responses of strains at 0.38 [m] from the origin of the two-link due to the base excitation

The above results show the validities of the formulation, computational codes and modeling the flexible two-link manipulator.

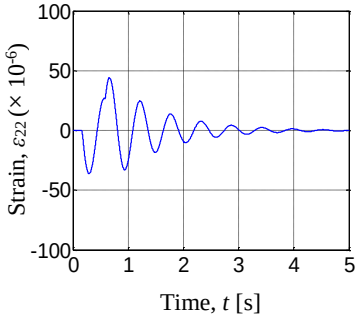

Fig. 15. Calculated time history responses of strains at Node 22 of Model *A* due to the base excitation

IV. Control Scheme

A control scheme to suppress the vibration of the single-link was designed using the piezoelectric actuator. It was done by adding bending moments generated by the piezoelectric actuator to the single-link. To drive the actuator, a PD-controller has been designed and examined through calculations and experiments.

The piezoelectric actuator suppresses the vibration of the two-link flexible manipulator by adding bending moments at nodes 3 and 6 of the two-link manipulator, M_3 and M_6. Therefore, the equation of motion of Link 1 become

$$\boldsymbol{M}_n\ddot{\boldsymbol{\delta}}_n + \boldsymbol{C}_n\dot{\boldsymbol{\delta}}_n + \left[\boldsymbol{K}_n - \dot{\theta}_1^{\,2}\boldsymbol{M}_n\right]\boldsymbol{\delta}_n = \ddot{\theta}_1\boldsymbol{f}_n + \boldsymbol{u}_n \tag{24}$$

where the vector of $\boldsymbol{u}_n$ containing M_3 and M_6 is the control force generated by the actuator to the two-link system.

Furthermore, substituting Eq. (19) to Eq. (18) gives

$$M_3 = -M_6 = \frac{d_1}{d_2}\varepsilon_1 \tag{25}$$

Based on Eq. (25), the bending moments can be defined in *s*-domain as follows

$$\boldsymbol{U}_n(s) = \boldsymbol{G}_C(s)\left(\varepsilon_d(s) - \varepsilon_6(s)\right) \tag{26}$$

where ε_d and ε_6 denote the desired and measured strains at Node 6, respectively.

A block diagram of the PD-controller for the two-link system is shown in Fig. 16.

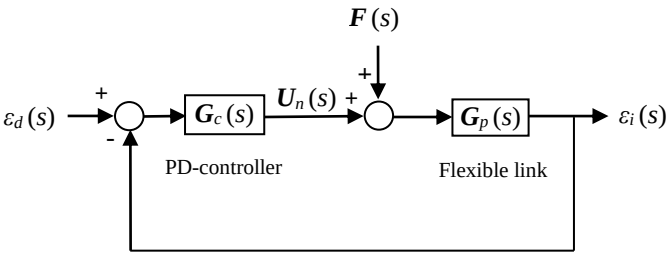

ε_d : Desired strain
$\boldsymbol{F}$: Base excitations
ε_i : Measured strains at Node i
$\boldsymbol{U}_n$: Applied bending moments

Fig. 16. Block diagram of proportional-derivative control of the flexible two-link manipulator

Moreover, the gain of PD-controller can be written by a vector in *s*-domain as follows

$$\boldsymbol{G}_C(s) = \begin{Bmatrix} 0 & 0 & 0 & K_p + K_d\, s & 0 & -\left(K_p + K_d\, s\right) & 0 & \cdots & 0 \end{Bmatrix}^T \tag{27}$$

V. Experiment

A. Experimental Set-up

In order to investigate the validity of the proposed control scheme, an experimental set-up was designed. The set-up is shown in Fig.17. The flexible two-link manipulator consists of two flexible aluminum beams, two clamp-parts, two servo motors and the base. Link 1 and Link 2 are attached to the first and second motors through the clamp-parts. Link 1 and Link 2 are connected through the second motor. In the experiments, the motors were operated by an independent motion controller. Two strain gages were bonded to the positions of 0.11 [m] and 0.38 [m] from the origin of the two-link system. An end-effector was introduced to the system in order to demonstrate a complete flexible two-link manipulator.

The piezoelectric actuator was attached on one side of Link 1 to provide the blocking force against vibrations. A Wheatstone bridge circuit was developed to measure the changes in resistance of the first strain gage in the form of voltages as feedback signals. An amplifier circuit was designed to amplify the small output signal of the Wheatstone bridge. Another Wheatstone bridge - amplifier circuits were used for the second strain gage.

Furthermore, a data acquisition board and a computer that have functionality of A/D (analog to digital) conversion, signal processing, control process and D/A (digital to analog) conversion were used. The data acquisition board connected to the computer through USB port. Finally, the controlled signals sent to a piezo driver to drive the piezoelectric actuator in its voltage range.

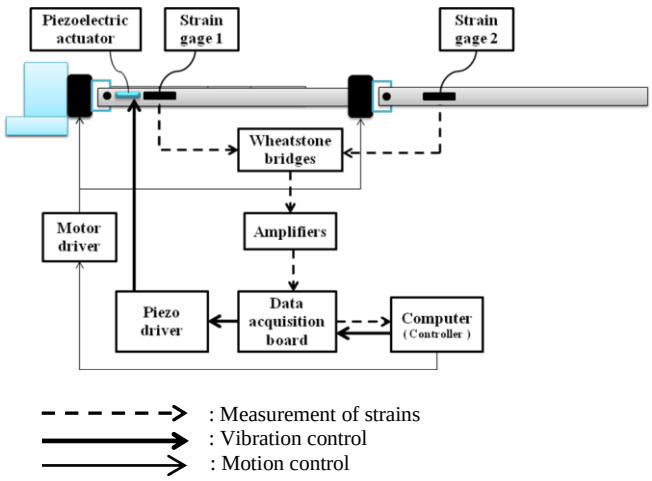

Fig. 17. Schematics of measurement and control system

B. Experimental Method

The rotations of the first and second motors were set from 0 to $\pi/4$ radians (45 degrees) and to $\pi/2$ radians (90 degrees) within 0.50 [s], respectively. Outputs of the first strain gage were converted to voltages by the Wheatstone bridge and magnified by the amplifier. The noises that occur in the experiment were reduced by a 100 [μF] capacitor attached to the amplifier. The output voltages of the amplifier sent to the data acquisition board and the computer for control process. The PD-controller was implemented in the computer using the visual C++ program. The analog output voltages of the data acquisition board sent to the input channel of the piezo driver to generate the actuated signals for the piezoelectric actuator.

VI. Calculated and Experimental Results

A. Calculated Results

Time history responses of strains on the uncontrolled and controlled systems were calculated when the first and second motors rotated by the angle of $\pi/4$ radian (45 degrees) and $\pi/2$ radians (90 degrees) within 0.50 [s], respectively. Time history responses of strains on the controlled system were calculated for Models *B* and *C* under the control scheme shown in Fig. 16. The concentrated mass m_c used for Model *C* is 14.49 [g].

Examining several gains of the PD-controller leaded to K_p = 2 [Nm] and K_d = 0.6 [Nms] as the better ones. Figures 18 and 20 show time history responses of strains at Node 2 and Node 22 for uncontrolled Model *B* while figures 19 and 21 show the controlled ones. The maximum and minimum strains of uncontrolled Model *B* at Node 6 in positive and negative sides were 984.30×10^{-6} and -878.40×10^{-6}, as shown in Fig. 18. By using PD-controller they became 430.00×10^{-6} and -453.50×10^{-6}, as shown in Fig. 19. Furthermore, the maximum and minimum strains of uncontrolled Model *B* at Node 22 in positive and negative sides were 58.55×10^{-6} and -53.37×10^{-6}, as shown in Fig. 20. By using PD-controller they became 36.27×10^{-6} and -39.13×10^{-6}, as shown in Fig. 21.

Moreover, figures 22 and 24 show time history responses of strains at Node 2 and Node 22 for uncontrolled Model *C* while figures 23 and 25 show the controlled ones.

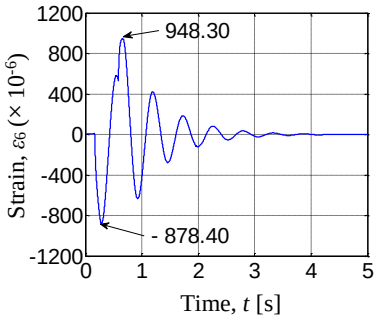

Fig. 18. Calculated time history response of strains at Node 6 for uncontrolled Model *B* due to the base excitations

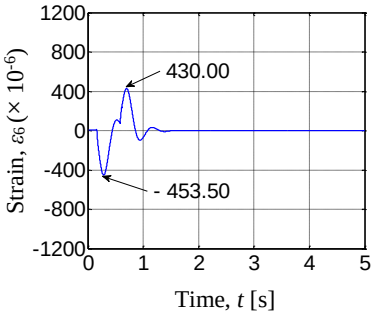

Fig. 19. Calculated time history response of strains at Node 6 for controlled Model *B* due to the base excitations (K_p = 2 [Nm] and K_d = 0.6 [Nms])

The maximum and minimum strains of uncontrolled Model *C* at Node 6 in positive and negative sides were 1388.00×10^{-6} and -1017.00×10^{-6}, as shown in Fig. 22. By using PD-controller they became 641.00×10^{-6} and -625.70×10^{-6}, as shown in Fig. 23. Furthermore, the maximum and minimum strains of uncontrolled Model *C* at Node 22 in positive and negative sides were 321.60×10^{-6} and -244.20×10^{-6}, as shown in Fig. 24. By using PD-controller they became 190.90×10^{-6} and -189.70×10^{-6}, as shown in Fig. 25.

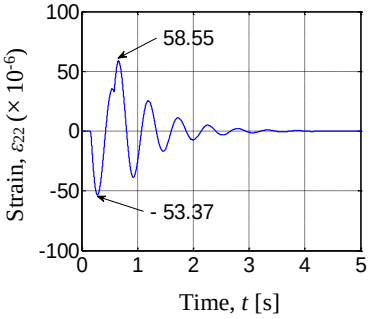

Fig. 20. Calculated time history response of strains at Node 22 for uncontrolled Model *B* due to the base excitations

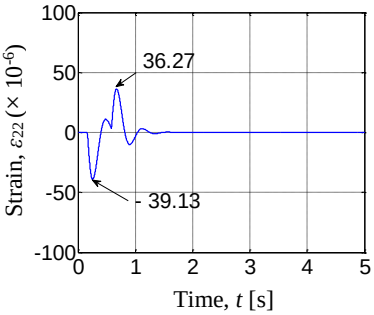

Fig. 21. Calculated time history response of strains at Node 22 for controlled Model *B* due to the base excitations (K_p = 2 [Nm] and K_d = 0.6 [Nms])

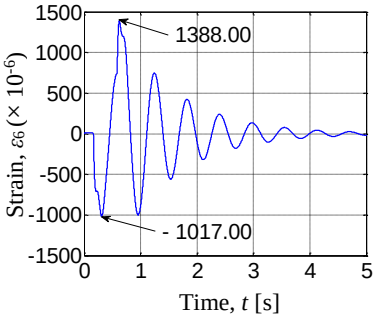

Fig. 22. Calculated time history response of strains at Node 6 for uncontrolled Model *C* due to the base excitations (m_c = 14.49 [g])

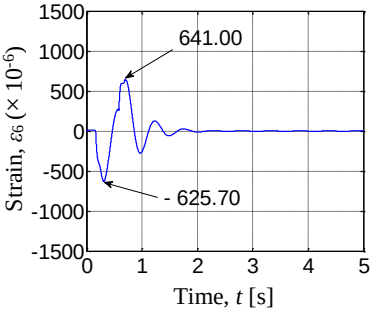

Fig. 23. Calculated time history response of strains at Node 6 for controlled Model *C* due to the base excitations (K_p = 2 [Nm], K_d = 0.6 [Nms] and m_c = 14.49 [g])

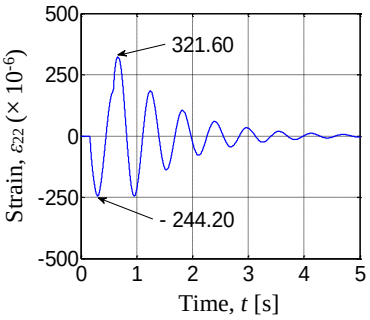

Fig. 24. Calculated time history response of strains at Node 22 for uncontrolled Model *C* due to the base excitations (m_c = 14.49 [g])

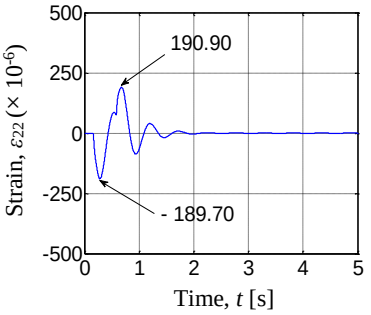

Fig. 25. Calculated time history response of strains at Node 22 for controlled Model *C* due to the base excitations (K_p = 2 [Nm], K_d = 0.6 [Nms] and m_c = 14.49 [g])

B. Experimental Results

Experiemental time history responses of strains on the uncontrolled and controlled systems were measured when the first and second motors rotated by the angle of $\pi/4$ radian (45 degrees) and $\pi/2$ radians (90 degrees) within 0.50 [s], respectively. Mass of the end-effector used in the experiments is 14.49 [g]. Time history responses of strains on the controlled system with and without the end-effector were measured under the control scheme shown in Fig. 16.

Several experimental gains of the PD-controller, K_p' (non-dimensional gain) and K_d' were examined. The examinations of gains leaded to K_p' = 300 [-] and K_d' = 0.3 [s] as the better ones. Figures 26 and 28 show time history responses of strains at positions of 0.11 [m] and 0.38 [m] from the link's origin for uncontrolled system without an end-effector while figures 27 and 29 show the controlled ones. The maximum and minimum strains of uncontrolled system without an end-effector at positions of 0.11 [m] from the link's origin in positive and negative sides were 954.10×10^{-6} and -836.60×10^{-6}, as shown in Fig. 26. By using PD-controller they became 613.10×10^{-6} and -644.10×10^{-6}, as shown in Fig. 27. Furthermore, the maximum and minimum strains of uncontrolled system without an end-effector at position of 0.38 [m] from the link's origin in positive and negative sides were 55.51×10^{-6} and -54.55×10^{-6}, as shown in Fig. 28. By using PD-controller they became 39.34×10^{-6} and -54.56×10^{-6}, as shown in Fig. 29.

Figures 30 and 32 show time history responses of strains at positions of 0.11 [m] and 0.38 [m] from the link's origin for uncontrolled system with the end-effector while figures 31 and 33 show the controlled ones. The maximum and minimum strains of uncontrolled system with the end-effector at positions of 0.11 [m] from the link's origin in positive and negative sides were 1298.00×10^{-6} and -1156.00×10^{-6}, as shown in Fig. 30. By using PD-controller

they became 1029.00×10^{-6} and -904.70×10^{-6}, as shown in Fig. 31. Furthermore, the maximum and minimum strains of uncontrolled system with the end-effector at positions of 0.38 [m] from the link's origin in positive and negative sides were 350.50×10^{-6} and -198.10×10^{-6}, as shown in Fig. 32. By using PD-controller they became 348.40×10^{-6} and -197.10×10^{-6}, as shown in Fig. 33.

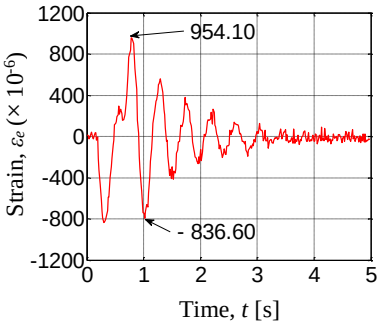

Fig. 26. Experimental time history responses of strains at 0.11 [m] from the link's origin for uncontrolled system without an end-effector due to the base excitations

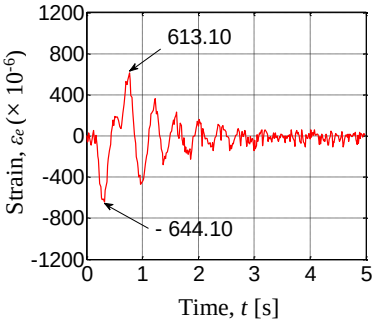

Fig. 27. Experimental time history responses of strains at 0.11 [m] from the link's origin for controlled system without an end-effector due to the base excitations (K_p' = 300 [-] and K_d' = 0.3 [s])

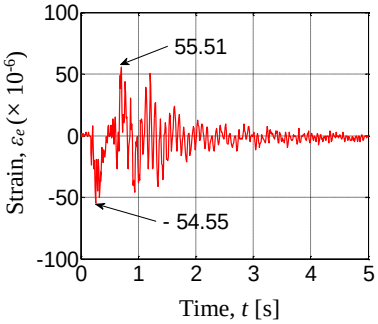

Fig. 28. Experimental time history responses of strains at 0.38 [m] from the link's origin for uncontrolled system without an end-effector due to the base excitations

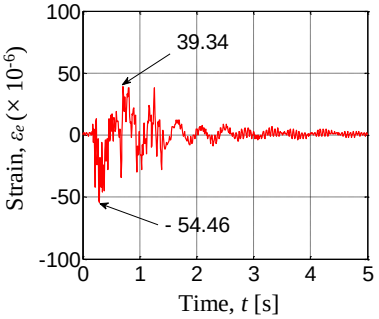

Fig. 29. Experimental time history responses of strains at 0.38 [m] from the link's origin for controlled system without an end-effector due to the base excitations (K_p' = 300 [-] and K_d' = 0.3 [s])

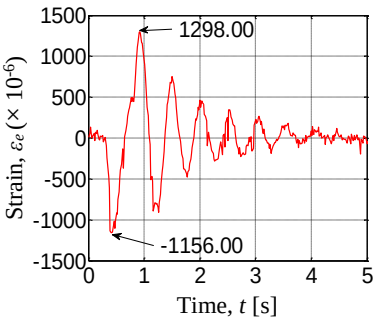

Fig. 30. Experimental time history responses of strains at 0.11 [m] from the link's origin for uncontrolled system with the end-effector due to the base excitations (m_c = 14.49 [g])

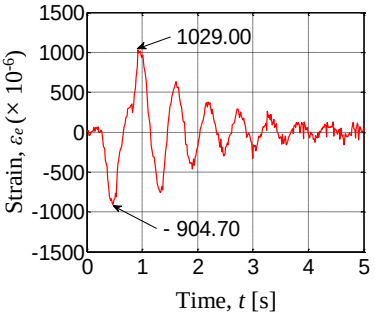

Fig. 31. Experimental time history responses of strains at 0.11 [m] from the link's origin for controlled system with the end-effector due to the base excitations (K_p' = 300 [-] and K_d' = 0.3 [s] and m_c = 14.49 [g])

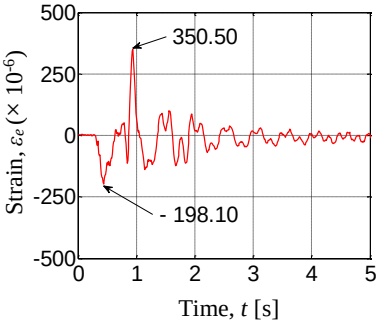

Fig. 32. Experimental time history responses of strains at 0.38 [m] from the link's origin for uncontrolled system with the end-effector due to the base excitations (m_c = 14.49 [g])

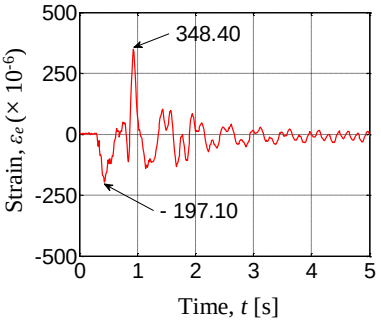

Fig. 33. Experimental time history responses of strains at 0.38 [m] from the link's origin for controlled system with the end-effector due to the base excitations (K_p' = 300 [-] and K_d' = 0.3 [s] and m_c = 14.49 [g])

It was verified from these results that the proposed control scheme can effectively suppress the vibration of the flexible two-link manipulator.

VII. Conclusion

The equations of motion for the flexible two-link manipulator had been derived using the finite-element method. Computational codes had been developed in order to perform dynamic simulations of the system. Experimental and calculated results on time history responses, natural frequencies and vibration modes show the validities of the formulation, computational codes and modeling of the system. The control scheme using a proportional-derivative (PD) controller was designed to suppress the vibration of the system. The proposed control scheme was examined through the calculations and experiments. The calculated and experimental results have revealed that the vibration of the flexible two-link manipulator can be suppressed effectively.

References

[1] C. Nishidome, and I. Kajiwara, "Motion and Vibration Control of Flexible-link Mechanism with Smart Structure", *JSME International Journal*, Vol.46, No.2, 2003, pp. 565 – 571.

[2] Y. Yaman et al, "Active Vibration Control of a Smart Beam", *Proceedings of the 2001 CANSMART Symposium*, 2001, pp. 125 – 134.

[3] O.F. Kircali et al, "Active Vibration Control of a Smart Beam by Using a Spatial Approach", *New Developments in Robotics, Automation and Control*, 2009, pp. 378 – 410.

[4] J. Zhang et al, "Active Vibration Control of Piezoelectric Intelligent Structures", *Journal of Computers*, Vol. 5. No. 3, 2010, pp. 401 – 409.

[5] K. Gurses et al, Vibration control of a single-link flexible manipulator using an array of fiber optic curvature sensors and PZT actuators, *Mechatronics* 19, 2009, pp. 167 – 177.

[6] S.X. Xu and T.S. Koko, "Finite Element Analysis and Design of Actively Controlled Piezoelectric Smart Structures", *Finite Elements in Analysis and Design* 40, 2004, pp. 241 – 262.

[7] Z.K. Kusculuoglu et al, "Finite Element Model of a Beam with a Piezoceramic Patch Actuator", *Journal of Sound and Vibration* 276, 2004, pp. 27 – 44.

[8] J.R. Hewit et al, "Active Force Control of a Flexible Manipulator by Distal Feedback", *Mech. Mach. Theory* Vol. 32, No. 5, 1997, pp. 583 – 596.

[9] A.R. Tavakolpour et al, "Modeling and Simulation of a Novel Active Vibration Control System for a Flexible Structures", *WSEAS Transaction on System and Control* Issue 5, Vol. 6, 2011, pp. 184 – 195.

[10] A.R. Tavakolpour and M. Mailah, "Control of Resonance Phenomenon in Flexible Structures Via Active Support", *Journal of Sound and Vibration* 331, 2012, pp. 3451 – 3465.

[11] A.K. Muhammad et al, "Computer Simulations on Vibration Control of a Flexible Single-link Manipulator Using Finite-element Method", *Proceeding of 19th International Symposium of Artificial Life and Robotics*, 2014, pp. 381 – 386.

[12] A.K. Muhammad et al, "Computer Simulations and Experiments on Vibration Control of a Flexible Link Manipulator Using a Piezoelectric Actuator", *Lecture Notes in Engineering and Computer Science: Proceeding of The International MultiConference of Engineers and Computer Scientists* 2014, IMECS 2014, 12 – 14 March, 2014, Hong Kong, pp. 262 – 267.

[13] A.K. Muhammad et al, "Comparison of Proportonal-derivative and Active-force Controls on Vibration of a Flexible Single-link Manipulator Using Finite-element Method", *Journal of Artificial Life and Robotics*, Vol. 19. No. 4, 2014, pp. 375 – 381.

[14] A.K. Muhammad et al, "Comparison of Proportonal and Active-force Controls on Vibration of a Flexible Link Manipulator Using a Piezoelectric Actuator through Calculations and Experiments", *Engineering Letters*, Vol. 22. No.3, 2014, pp. 134 – 141.

[15] A.K. Muhammad et al, "Active-force Controls on Vibration of a Flexible Single-link Manipulator Using a Piezoelectric Actuator", in *Transactions on Engineering Technologies: International MultiConference of Engineers and Computer Scientists* 2014, G.-C. Yang et al, Ed. Springer, 2014, pp. 1 – 15.

[16] M. Lalanne et al, *Mechanical Vibration for Engineers*, John Wiley & Sons Ltd, 1983, pp. 146 – 153.

[17] www.mmech.com, *Resin Coated Multilayer Piezoelectric Actuators.*